Optical bistability in semiconductor microcavities

A. Baas,[1] J. Ph. Karr,[1] H. Eleuch,[2] and E. Giacobino[1]
[1]*Laboratoire Kastler Brossel, Université Paris 6, Ecole Normale Supérieure et CNRS, UPMC Case 74, 4 place Jussieu, 75252 Paris Cedex 05, France*
[2]*Institut National des Sciences Appliquées et de Technologie, Centre Urbain Nord Bp N 676, 1080 Tunis Cedex, Tunisia*
(Received 1 July 2003; published 17 February 2004)

We report the observation of polaritonic bistability in semiconductor microcavities in the strong-coupling regime. The origin of bistability is the polariton-polariton interaction, which gives rise to a Kerr-like nonlinearity. The experimental results are in good agreement with a simple model taking transverse effects into account.

DOI: 10.1103/PhysRevA.69.023809 PACS number(s): 42.65.Pc, 71.36.+c, 78.67.−n, 42.50.−p

I. INTRODUCTION

In high finesse semiconductor microcavities with embedded quantum wells, the demonstration of the strong-coupling regime between the quantum well excitons and the cavity photons [1] has opened the way to a refined manipulation of a new species, cavity polaritons, that are mixed light-matter eigenstates [2]. While strong-coupling or normal-mode coupling appears for very small photon numbers, polaritons exhibit a number of nonlinear behaviors [3]. Polariton bleaching has been observed at high excitation density [4] and is predicted to give rise to optical bistability [5]. With intermediate excitation densities for which strong coupling still exists, these systems exhibit strong nonlinear emission, due to parametric polariton amplification. The nonlinearity comes from the exciton part of the polariton through coherent exciton-exciton scattering.

The polariton scattering must fulfil phase-matching conditions for the in-plane wave vector of the considered polaritons. If $\mathbf{k}_P$ is the wave vector of the excitation, two polaritons with wave vector $\mathbf{k}_P$ scatter to give polaritons with wave vectors $\mathbf{0}$ and $\mathbf{2k}_P$. In addition, energy conservation implies that $E(0)+E(2k_p)=2E(k_P)$. Most of the experiments on the polariton parametric amplification have been performed in the magic angle configuration [6,8], where k_P is the nontrivial solution for the energy conservation condition. However, there also exists a trivial solution $\mathbf{k}_P=\mathbf{0}$ where only the $\mathbf{k}=\mathbf{0}$ mode is involved. In this case, in the same way as in degenerate parametric amplification, polaritonic wave mixing gives rise to phase dependent amplification [9] and eventually to polariton squeezing [10].

In this geometry of excitation, the effective Hamiltonian (at first order) for the polariton-polariton interaction [11,12] is analogous to the Hamiltonian of an optical Kerr medium. The difference is that the refraction index depends on the polariton number instead of the photon number. This gives rise to a bistable behavior for high enough excitation intensities, in the same way as for a Kerr medium in a cavity. Optical bistability has already been observed in quantum well microcavities in the weak-coupling regime [13]; it has been predicted to occur in the strong-coupling regime due to exciton bleaching [5], however in different conditions.

In this paper we give experimental evidence for a bistable behavior in a microcavity sample in the strong-coupling regime. To our knowledge, this is the first observation of bistability in the strong-coupling regime. We also investigate the nonlinear patterns that appear in the transverse plane. We show that the main features of the experimental results can be explained satisfactorily by treating the polariton-polariton interaction at first order, i.e., in terms of a polariton Kerr effect.

The paper is organized as follows. In Sec. I, we give the effective Hamiltonian for the polariton system, using the same set of hypotheses that has been used for the study of the ''magic angle'' configuration [11,12]. We establish the evolution equation for the polariton field, and we solve the steady-state regime in order to compute the bistability threshold, as well as the reflectivity and transmission spectra. Section II is the experimental study of the bistability regime. We show that it is necessary to take transverse effects into account and we compare the experimental results with the prediction of the model studied in Sec. I, including a simple treatment of the transverse effects.

II. MODEL

A. Hamiltonian

The linear Hamiltonian for excitons and cavity photons is $H=\Sigma_{\mathbf{k}}H_{\mathbf{k}}$ with [14]

$$H_{\mathbf{k}}=E_{exc}(k)b_{\mathbf{k}}^{\dagger}b_{\mathbf{k}}+E_{cav}(k)a_{\mathbf{k}}^{\dagger}a_{\mathbf{k}}+\frac{\Omega_R}{2}(a_{\mathbf{k}}^{\dagger}b_{\mathbf{k}}+b_{\mathbf{k}}^{\dagger}a_{\mathbf{k}}). \tag{1}$$

In this equation $a_{\mathbf{k}}$ and $b_{\mathbf{k}}$ are the creation operators for photons and excitons with a wave vector $\mathbf{k}$ in the layer plane. Because of the translational invariance in the cavity plane, photons can only interact with excitons having the same $\mathbf{k}$. $E_{cav}(k)$ $[E_{exc}(k)]$ is the cavity (exciton) dispersion and Ω_R is the Rabi interaction energy between excitons and photons. The normal modes of the linear Hamiltonian $H_{\mathbf{k}}$ are called cavity polaritons. The annihilation operators $p_{\mathbf{k}}$, and $q_{\mathbf{k}}$ for the lower and upper polaritons are given by

$$p_{\mathbf{k}}=X_k b_{\mathbf{k}}-C_k a_{\mathbf{k}}, \tag{2}$$

$$q_{\mathbf{k}}=C_k b_{\mathbf{k}}+X_k a_{\mathbf{k}}, \tag{3}$$

where X_k and C_k are the Hopfield coefficients [15] given by

$$X_k=\left(\frac{\delta_k+\sqrt{\delta_k^2+\Omega_R^2}}{2\sqrt{\delta_k^2+\Omega_R^2}}\right)^{1/2}, \tag{4}$$

$$C_k=\left(\frac{\Omega_R^2}{2\sqrt{\delta_k^2+\Omega_R^2}(\delta_k+\sqrt{\delta_k^2+\Omega_R^2})}\right)^{1/2}, \tag{5}$$

with $\delta_k=E_{cav}(k)-E_{exc}(k)$. In the polariton basis, the linear Hamiltonian reads

$$H_{\mathbf{k}}=E_{LP}(k)p_{\mathbf{k}}^{\dagger}p_{\mathbf{k}}+E_{UP}(k)q_{\mathbf{k}}^{\dagger}q_{\mathbf{k}}, \tag{6}$$

where $E_{LP}(k)$ [$E_{UP}(k)$] is the lower (upper) polariton dispersion given by

$$E_{LP(UP)}(k)=E_{exc}(k)+\frac{\delta_k}{2}-(+)\frac{1}{2}\sqrt{\delta_k^2+\Omega_R^2}. \tag{7}$$

The Coulomb interaction between the carriers gives rise to two additional terms: an effective exciton-exciton interaction term and an anharmonic saturation term in the light-exciton coupling. The exciton-exciton interaction term is

$$H_{exc\text{-}exc}=\frac{1}{2}\sum_{\mathbf{k},\mathbf{k}',\mathbf{q}}V_q b_{\mathbf{k}+\mathbf{q}}^{\dagger}b_{\mathbf{k}'-\mathbf{q}}^{\dagger}b_{\mathbf{k}}b_{\mathbf{k}'}, \tag{8}$$

with $V_q\simeq V_0=6e^2a_{exc}/\epsilon_0 A$, provided $qa_{exc}\ll 1$ [11,16], a_{exc} being the two-dimensional Bohr radius of the exciton, ϵ_0 the dielectric constant of the quantum wells, and A the quantization area. The saturation term is written as

$$H_{sat}=-\sum_{\mathbf{k},\mathbf{k}',\mathbf{q}}V_{sat}(a_{\mathbf{k}+\mathbf{q}}^{\dagger}b_{\mathbf{k}'-\mathbf{q}}^{\dagger}b_{\mathbf{k}}b_{\mathbf{k}'}+a_{\mathbf{k}+\mathbf{q}}b_{\mathbf{k}'-\mathbf{q}}b_{\mathbf{k}}^{\dagger}b_{\mathbf{k}'}^{\dagger}), \tag{9}$$

with $V_{sat}=\Omega_R/2n_{sat}A$ [11,16], where $n_{sat}=7/(16\pi a_{exc}^2)$ is the exciton saturation density. As long as the nonlinear terms are small compared to the Rabi splitting Ω_R, it is possible to neglect the nonlinear interaction between the upper and lower branches, which yields nonsecular terms. The two polaritons are then virtually decoupled and it is more appropriate to use the polariton basis. In addition, we consider a resonant excitation of the lower branch by a quasimonochromatic laser field and we will focus our attention on the evolution of the lower branch polariton. In terms of the lower polariton operator the Hamiltonian is $H=H_{LP}+H_{PP}^{eff}$. The free polariton term is $H_{LP}=\Sigma_{\mathbf{k}}E_{LP}(k)p_{\mathbf{k}}^{\dagger}p_{\mathbf{k}}$. The effective polariton-polariton interaction term is

$$H_{PP}^{eff}=\frac{1}{2}\sum_{\mathbf{k},\mathbf{k}',\mathbf{q}}V_{\mathbf{k},\mathbf{k}',\mathbf{q}}^{PP}p_{\mathbf{k}+\mathbf{q}}^{\dagger}p_{\mathbf{k}'-\mathbf{q}}^{\dagger}p_{\mathbf{k}}p_{\mathbf{k}'}, \tag{10}$$

with

$$V_{\mathbf{k},\mathbf{k}',\mathbf{q}}^{PP}=V_0X_{|\mathbf{k}'-\mathbf{q}|}X_kX_{|\mathbf{k}+\mathbf{q}|}X_{k'}+2V_{sat}X_{|\mathbf{k}'-\mathbf{q}|}X_k(C_{|\mathbf{k}+\mathbf{q}|}X_{k'}+C_{k'}X_{|\mathbf{k}+\mathbf{q}|}). \tag{11}$$

For the typical parameters $\Omega_R=3$ meV, $a_{exc}=100$ Å and $\epsilon_0=(3.5)^2\epsilon_0^{vacuum}$ we find $V_{sat}/V_0\simeq 0.012$. Therefore in Eq. (11) we can neglect the saturation term with respect to the Coulomb interaction term (except for the case of an extreme negative detuning, where one can have $C_k\gg X_k$):

$$V_{\mathbf{k},\mathbf{k}',\mathbf{q}}^{PP}\simeq V_0X_{|\mathbf{k}+\mathbf{q}|}X_{k'}X_{|\mathbf{k}'-\mathbf{q}|}X_k. \tag{12}$$

In the following we consider a resonant excitation at normal incidence (in the $\mathbf{k}=0$ direction) and we study the reflected field (again in the $\mathbf{k}=0$ direction). In this case the interaction of the $\mathbf{k}=0$ polaritons with other modes gives rise to the collision broadening calculated by Ciuti in Ref. [16]. He predicted a threshold behavior of the broadening. The exciton density at threshold is $n_{exc}=7\times10^9$ cm^{-2} at $\delta=3$ meV for a sample with a Rabi splitting $\Omega=3$ meV. Below this threshold, we can neglect the collision broadening and keep only the lowest-order term. Only a Kerr-like nonlinear term remains:

$$H_{PP}^{eff}=\tfrac{1}{2}V_{\mathbf{0}}p_{\mathbf{0}}^{\dagger}p_{\mathbf{0}}^{\dagger}p_{\mathbf{0}}p_{\mathbf{0}}. \tag{13}$$

Finally we include a term describing the coupling between the cavity mode and the external pump field of frequency ω_L, treated as a classical field with amplitude A^{in} [17]:

$$H_{pump}=i\hbar\sqrt{2\gamma_1}[A^{in}\exp(-i\omega_Lt)a^{\dagger}-\text{H.c.}], \tag{14}$$

where γ_1 the dissipation coefficient of the front mirror of the cavity.

B. Evolution equation

From the Hamiltonian $H=H_{LP}+H_{PP}^{eff}+H_{pump}$ it is now easy to derive the Heisenberg equation for the $\mathbf{k}=0$ lower polariton operator $p_{\mathbf{0}}$ (renamed as p in the following). The relaxation is treated phenomenologically by adding a loss term. The associated fluctuation terms are not included. This treatment is suitable only for the study of the mean stationary values of the fields. One obtains

$$\frac{dp}{dt}=-(\gamma_p+i\delta_p)p-i\alpha_pp^{\dagger}pp-C_0\sqrt{2\gamma_1}A^{in}, \tag{15}$$

where $\delta_p=E_{LP}(0)/\hbar-\omega_L$ is the frequency detuning between the polariton resonance and the laser. γ_p is the polariton linewidth, given in a simple coupled oscillator model by $\gamma_p=C_0^2\gamma_a+X_0^2\gamma_b$ where γ_a and γ_b are the bare cavity and exciton linewidths, respectively. This gives correct values of the linewidth at low excitation density for a limited range of detunings around zero detuning. At higher excitation the collision broadening should be taken into account. α_p is the polariton effective nonlinear coefficient given by

$$\alpha_p=\frac{X_0^4V_0}{\hbar}. \tag{16}$$

Equation (15) will be our starting point for the study of the nonlinear effects. It is analogous to the evolution equation of the optical field in a cavity containing an ideal passive

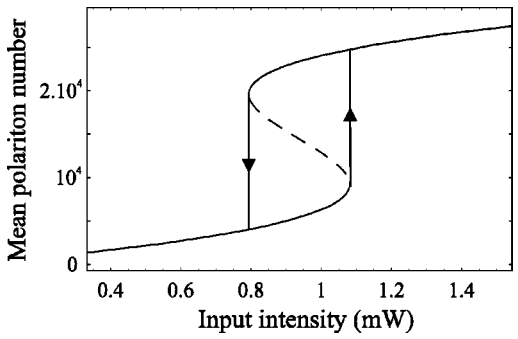

FIG. 1. Intensity of the polariton field (i.e., the mean number of polaritons n_p) vs the input power I^{in} in milliwatts. The nonlinear coefficient is $V_0=4.5\times10^{-5}$ meV (corresponding to a spot of 50 μm in diameter). The cavity and exciton linewidths are $\gamma_a=0.12$ meV and $\gamma_b=0.075$ meV and the polariton linewidth is taken as equal to $\gamma_p=C_0^2\gamma_a+X_0^2\gamma_b$ (see text). The cavity-exciton detuning is $\delta=0$. The laser detuning is $\delta_p=-2.5\gamma_p$. In the bistable region, the dotted line is the unstable branch. The arrows indicate the hysteresis cycle obtained by scanning the input power in both directions.

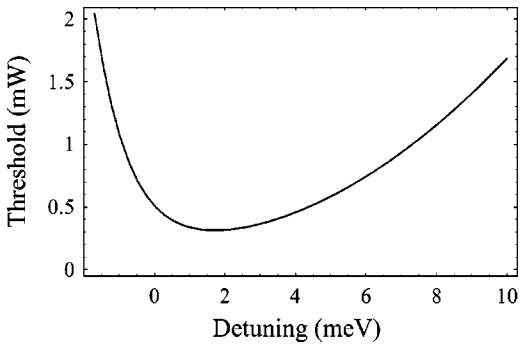

FIG. 2. Variations of the bistability threshold in milliwatts vs the cavity-exciton detuning. The parameters are the same as in Fig. 1.

Kerr medium. It is therefore expected that the nonlinear polariton system should exhibit bistability. Let us note that our system is made more complex by the composite nature of the cavity polaritons. All the parameters, such as the polariton linewidth, the nonlinear coefficient and the coupling to radiation are functions of the cavity-exciton detuning, which determines the photon and exciton contents of the polariton.

C. Steady-state regime

We rewrite Eq. (15) for the mean fields and we solve the stationary regime:

$$\frac{d\langle p\rangle}{dt}=-(\gamma_p+i\delta_p)\langle p\rangle-i\alpha_p n_p\langle p\rangle-C_0\sqrt{2\gamma_1}\langle A^{in}\rangle=0, \tag{17}$$

where $n_p=|\langle p\rangle|^2$ is the mean number of polaritons. Multiplying Eq. (17) by its conjugate, we obtain an equation for n_p:

$$n_p[\gamma_p^2+(\delta_p+\alpha_p n_p)^2]=2\gamma_1 C_0^2 I^{in}. \tag{18}$$

The plot of n_p versus the excitation power shows a bistable behavior for certain values of δ_p, as can be seen in Fig. 1. For a range of values of the driving laser power the polariton number is found to have two possible values, located on the higher and the lower stable branches of the curve (the intermediate branch is well known to be unstable). The turning points are given by the equation $dI^{in}/dn_p=0$:

$$3\alpha_p^2 n_p^2+4\alpha_p n_p\delta_p+\gamma_p^2+\delta_p^2=0. \tag{19}$$

The discriminant of this equation is written as

$$\Delta=\alpha_p^2(\delta_p^2-3\gamma_p^2). \tag{20}$$

A bistable behavior is obtained for positive values of the discriminant, i.e., $\delta_p^2>3\gamma_p^2$. Moreover the solutions for n_p should be positive real numbers. Combining these two conditions, bistability is obtained when

$$\delta_p<-\sqrt{3}\gamma_p, \quad \text{i.e.,} \quad \omega_L>\omega_p+\sqrt{3}\gamma_p. \tag{21}$$

In this case, the value of n_p corresponding to the bistability turning point is written as

$$n_p^1=\frac{-2\delta_p-\sqrt{\delta_p^2-3\gamma_p^2}}{3\alpha_p} \tag{22}$$

and one can simply obtain from Eq. (18) the corresponding threshold for the excitation intensity:

$$I^{in}=\frac{-(2\delta_p+\sqrt{\delta_p^2-3\gamma_p^2})}{27\alpha_p C_0^2\gamma_1}(\delta_p^2+3\gamma_p^2-\delta_p\sqrt{\delta_p^2-3\gamma_p^2}). \tag{23}$$

D. Bistability threshold

The lowest threshold is obtained when the detuning between the laser and the polariton resonance δ_p is equal to $-\sqrt{3}\gamma_p$. The corresponding threshold is

$$I_{thr}^{in}=\frac{4\gamma_p^3}{3\sqrt{3}\alpha_p C_0^2\gamma_1}. \tag{24}$$

It is interesting to study the variations of the threshold with the cavity-exciton detuning δ. Using Eqs. (4), (5), and (16) to replace X_0, C_0, and α_p, the threshold can be written as

$$I_{thr}^{in}=\frac{8[\delta^2\gamma_b+2(\gamma_a+\gamma_b)g^2+\delta\gamma_b\sqrt{\delta^2+4g^2}]^3}{[3\sqrt{3}g^2(\delta+\sqrt{\delta^2+4g^2})^4\alpha_{exc}\gamma_1]}. \tag{25}$$

The variations of the threshold versus the cavity-exciton detuning are shown in Fig. 2. The threshold intensity is found to reach a minimum value for the detuning δ_0 given by

$$\delta_0=\frac{2\gamma_a-\gamma_b}{\sqrt{2\gamma_a\gamma_b}}g. \tag{26}$$

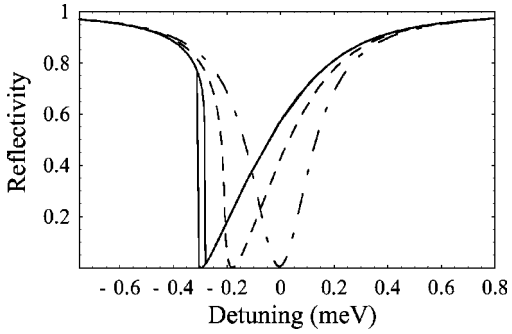

FIG. 3. Reflectivity spectra as a function of the cavity-exciton detuning for I^{in} near zero (dash-dotted line), $I^{in}=0.5$ mW (dashed line), and $I^{in}=1$ mW (solid line). The laser energy is $E_L=E_{exc}-\Omega_R/2$, equal to the lower polariton energy at zero cavity-exciton detuning in the absence of nonlinear effects. The other parameters are the same as in Fig. 1. The reflectivity resonance is indeed at $\delta=0$ in the low intensity case but it is shifted at higher intensity. For the highest intensity, a hysteresis cycle appears when scanning the spot position in the two directions.

With the parameters of Fig. 2 we find $\delta_0=1.72$ meV. As explained in the preceding section, the optical response of the system is governed by the composite nature of the polariton, with exciton and photon fractions depending on the cavity-exciton detuning. The value δ_0 of the detuning is the result of a trade-off between coupling to the external radiation (which is stronger for negative detuning, when the polariton tends to a photon) and nonlinearity (which is stronger for positive detuning, when the polariton tends to an exciton).

E. Reflectivity and transmission spectra

In this section we compute the reflectivity, absorption, and transmission spectra, which show hysteresis cycles above the bistability threshold.

The reflectivity and transmission coefficients are obtained in the following way. First we compute the stationary mean value p_0 of the intracavity polariton field using Eq. (17). Then we compute the mean value of the intracavity photon field using Eqs. (2) and (3) and the fact that the upper polariton field q is set to zero, which yields the simple relationship $a=-C_0p$. Finally the reflected and transmitted fields are calculated using the input-output relationships $A_i^{out}=\sqrt{2\gamma_i}a-A_i^{in}$ for $i=1,2$. The coefficients R, T, and A are given, respectively, by I_1^{out}/I^{in}, I_2^{out}/I^{in}, and $1-R-T$.

Bistability can be evidenced by scanning the input intensity for a fixed detuning between the exciton and the cavity. Alternatively, it is possible to scan the cavity length for a fixed value of the input intensity, as for atoms in cavity [18]. In a semiconductor microcavity, this can be done by scanning the excitation spot on the sample surface, since the cavity is wedged (i.e., there is a slight angle between the Bragg mirrors).

Figure 3 shows the variations of R with the cavity-exciton detuning for three values of I^{in} (close to zero, below, and above the bistability threshold). For the highest intensity, the reflectivity spectrum shows the characteristic hysteresis cycle. The output power switches abruptly when the position of the excitation spot is scanned; in the bistable region the output power depends on the direction of the scan. The hysteresis cycle can also be seen on the transmission and absorption spectra.

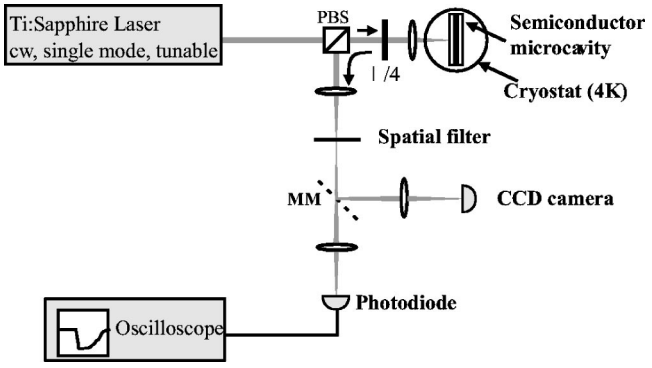

FIG. 4. Experimental setup. The microcavity sample is excited using a Ti:sapphire laser. The quarter-wave plate in front of the sample ensures excitation with a circular polarization. The polarizing beam splitter (PBS) and the quarter-wave plate form an optical circulator that separates the reflected light from the excitation beam. A spatial filter is placed in the near field of the reflected beam. Using the movable mirror MM, the beam can be either observed on a CCD camera, again in the near field (which allows one to study the spatial effects and to choose the position of the spatial filter), or sent towards a photodiode.

Thus our theoretical model shows that the exciton-exciton interaction in semiconductor microcavities leads to an optically bistable regime in the frequency region of the polariton resonance. An alternative mechanism for achieving optical bistability was proposed in Ref. [5], using the bleaching of the Rabi splitting; in contrast with this case, we obtain the present effect when the exciton-exciton interaction term is much smaller than the Rabi splitting term. We also stress that this mechanism is different from the optical bistability which has been demonstrated in semiconductor microcavities at room temperature [13], since it involves an exciton-photon mixed mode instead of a cavity mode.

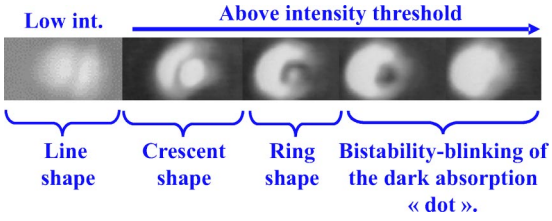

FIG. 5. Near-field images of the reflected beam. The laser wavelength is 831.69 nm, resonant with the lower polariton at $\delta=0.3$ meV. The first image is taken at very low excitation intensity (0.2 mW). All the other images are taken at 2 mW, for different positions of the excitation spot on the sample. The last two images are obtained for the same position; we observed a blinking between these two states, due to mechanical vibrations.

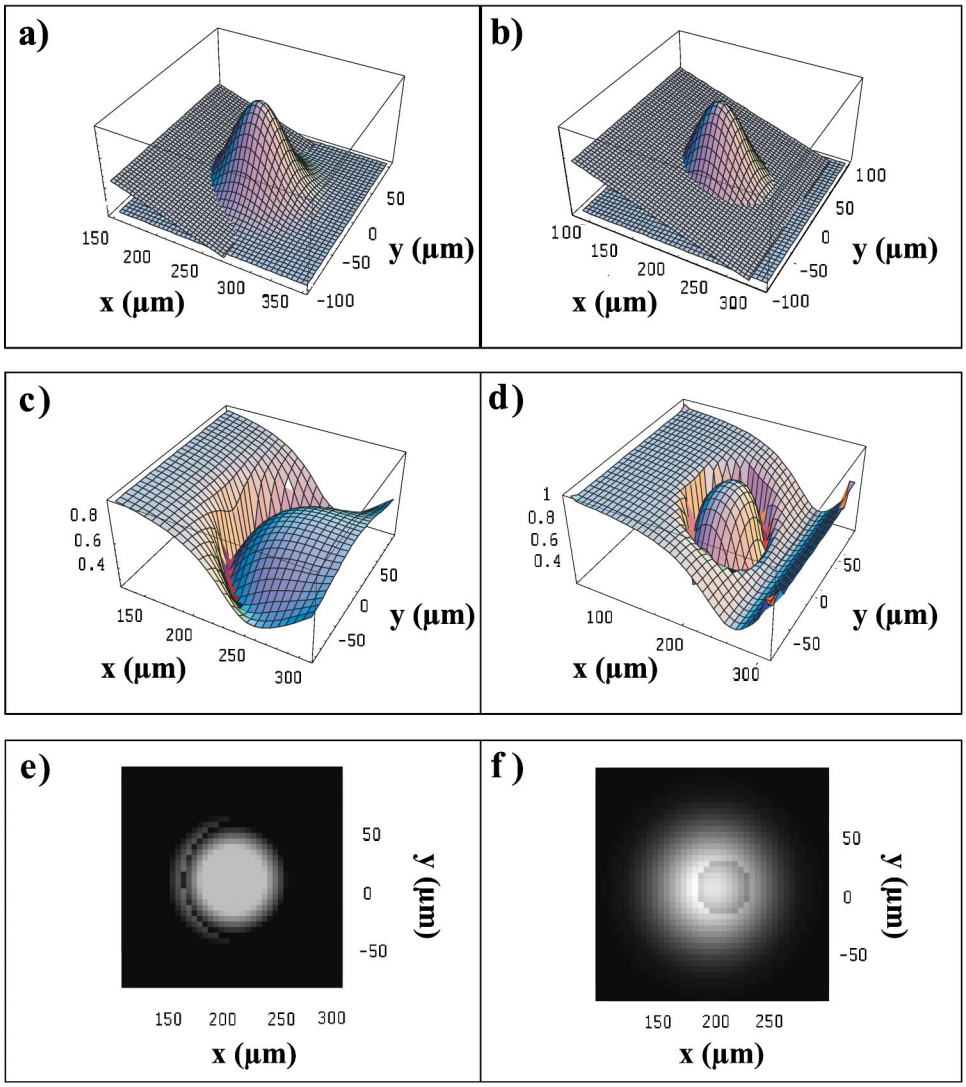

FIG. 6. All curves are drawn as a function of the position (x,y) in the transverse plane. (a), (b) Nonlinear energy shift proportional to the Gaussian intensity distribution of the excitation spot and linear shift due to the cavity wedge for two positions of the spot on the sample: $X=245$ μm and $X=180$ μm ($X=0$ corresponds to zero exciton-cavity detuning). (c) and (d) represent reflectivity for the parameters of (a) and (b), respectively. The reflectivity resonance is obtained when the nonlinear shift compensates exactly for the linear shift, i.e., at the intersections between the two curves of (a) and (b). The low-intensity resonance (a straight line) can be seen on the edge of (d). (e) and (f) represent near-field images of the spot for the parameters of (a) and (b), respectively, obtained by convolution of the reflectivity with the intensity distribution. They are to be compared with the first two pictures in Fig. 5. Note that the low-intensity resonance region of (d) is not visible in (f) since the local intensity is very low. The unshifted resonance is at $X=270$ μm.

III. EXPERIMENTAL RESULTS

The experimental setup is shown in Fig. 4. The microcavity sample consists of one $In_{0.05}Ga_{0.95}As$ quantum well embedded in a λ GaAs spacer, sandwiched between 20 (26.5) pairs of $Ga_{0.9}Al_{0.1}As/AlAs$ distributed Bragg reflectors on top (bottom). The linewidths (full width at half maximum) of the bare exciton and cavity modes are, respectively, 0.15 meV and 0.24 meV, and the Rabi splitting is $\Omega_R = 2.8$ meV. The sample is held in a cold-finger cryostat at a temperature of 4 K. The cavity has a slight wedge which allows to tune the cavity length by scanning the position of excitation on the sample. The light source is a single-mode tunable cw Ti:sapphire laser with a linewidth of the order of 1 MHz. The laser beam is power stabilized by means of an electro-optic modulator and spatially filtered by a 2 m long single-mode fiber. The spot diameter is 50 μm. In all experiments the lower polariton branch was excited near resonance at normal incidence with a σ^+ polarized beam.

The image of the excitation spot on the sample surface is made on a charge-coupled device (CCD) camera. Indeed spatial effects are important in our system. On the one hand, due to the slight angle between the cavity mirrors the polariton energy depends linearly on the position; on the other hand the nonlinearity gives rise to spatial patterns due to the Gaussian intensity distribution in the laser spot. Transverse effects are thus critical for the understanding of the optical

response of the sample and, we will now present their experimental study.

A. Transverse effects

1. Near-field images

We first studied the near field of the reflected beam. At sufficiently low excitation intensity, the spot shows a dark vertical line corresponding to absorption occurring on the polariton resonance. The variation of absorption with the position is due to the slight angle between the cavity mirrors, and the dark line is a line of equal thickness of the microcavity. At higher laser intensities, even well below the bistability threshold, one observes a strong distortion of the resonance line as shown in Fig. 5. When scanning the spot position on the sample (which amounts to scanning the polariton energy) one can see a change from a crescent shape to a ring shape, and then to a dot shape.

2. Theoretical study

In order to understand these results we have computed the reflectivity of the microcavity in the transverse plane, taking both the Gaussian intensity distribution of the excitation spot and the wedged shape of the cavity into account. The excitation spot is discretized into small spots with different local excitation densities and local cavity thicknesses. The pixels are assumed to be uncorrelated to each other. For each spot we compute the reflectivity from Eq. (15). This is the simplest possible treatment, which includes neither the transverse mode structure of the microcavity [19] (since it is based on a plane-wave approximation) nor the effect of diffraction. However it gives a good qualitative understanding of the shape of the absorption region.

At low intensity, the resonance region is found to be a straight line, as observed in the experiments. The results at higher intensity with the experimental parameters of Fig. 5 can be seen in Fig. 6 for two different positions of the excitation spot. The main resonant region can be seen near the center of the spot; depending on the position of the spot, its shape is that of a crescent, a ring, or a dot, in good agreement with the experimental results. The shape of the resonance region can be understood as resulting from exact compensation between the nonlinear energy shift due to the intensity variations and the linear energy shift due to the cavity thickness variations. The results of Fig. 6 are in good agreement with the first two pictures of Fig. 5 that correspond to the same parameters. The blinking of the dark absorption dot as a whole in the bistable region cannot be reproduced by our model, because it is linked to the spatial coherence over the size of the dot (i.e., the size of the polariton mode), while in our model there are no spatial correlations between the pixels used in the calculation.

B. Reflectivity spectra

In view of these transverse effects, the interpretation of the reflectivity spectrum will be much simpler if we select a small zone on the sample in order to avoid averaging the optical response on the spot surface. One solution would be to have an excitation spot with a uniform distribution in intensity, sufficiently small so that the cavity wedge would be negligible. Spatial selection can be also easily achieved by spatial filtering of the reflected beam. We used a spatial filter for the reflected light in order to select only a small fraction of the excitation spot. The filter has the size of the dark absorption dot of Fig. 5, i.e., about 10 μm in diameter.

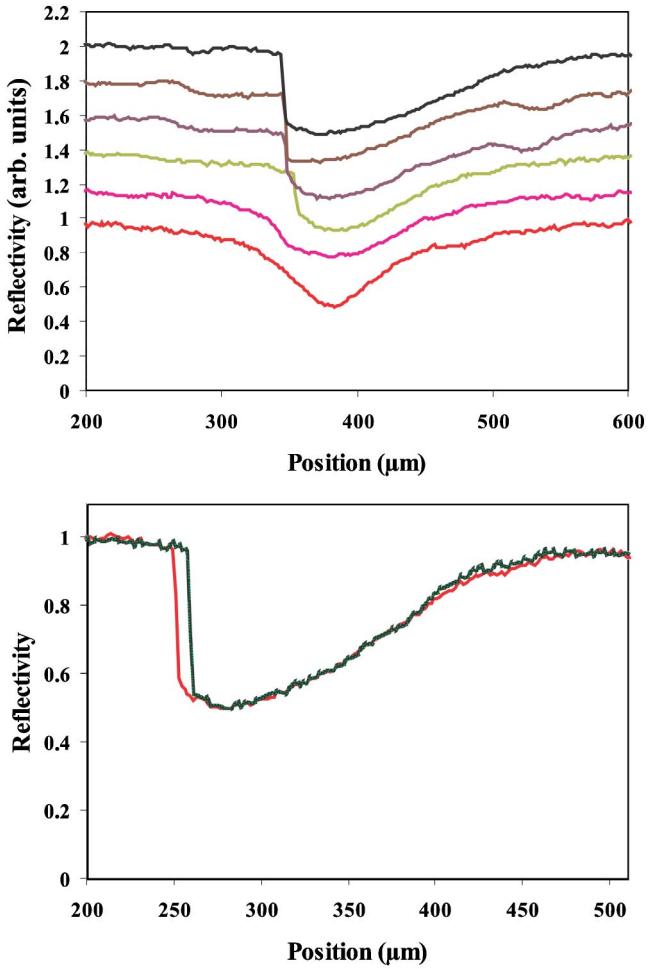

FIG. 7. Upper figure: reflected intensities (in arbitrary units) as a function of the spot position on the sample (the origin of the axis is arbitrary), for several values of the input power I^{in}: 1, 2, 3, 4, 5, and 6 mW. The laser wavelength is 831.32 nm, resonant with the lower polariton at $\delta=1.5$ meV. Bistability appears at $I^{in}=2.8$ mW. Lower figure: hysteresis cycle for the curve $I^{in}=6$ mW. The two curves correspond to the two directions for the scan of the spot position on the sample.

Two photodiodes allow to measure the reflected and transmitted intensities. Each spectrum is obtained at fixed excitation energy and intensity, by scanning the spot position over the sample surface. This is equivalent to a scan of the cavity length. As a result, the precision of the measurements is limited by the surface defects of the sample. Figure 7 shows a series of spectra for several values of the excitation intensity.

We observed a shift of the resonance position, which is proportional to the excitation intensity (see Fig. 8). The resonance position shifts towards negative detunings, corresponding to a blue shift of the resonance energy. This is in

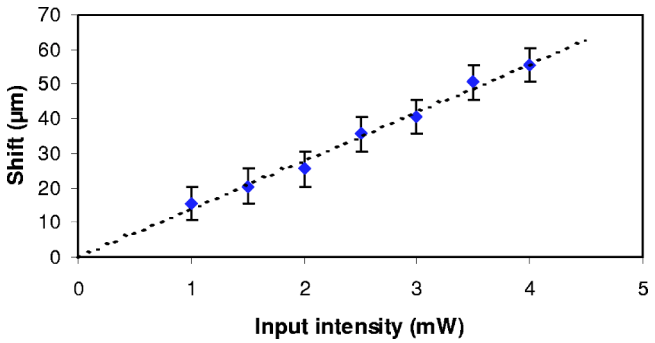

FIG. 8. Shift of the reflectivity minimum on the sample as a function of the input power. The laser wavelength is 831.32 nm, resonant with the lower polariton at $\delta = 1.5$ meV.

agreement with the model, where the blue shift is given by the effective Hamiltonian (13). The shift has been removed in Fig. 7, so that all the curves appear to be peaked around the same position.

Above a threshold intensity, one can observe as expected an hysteresis cycle by scanning the sample position in the two directions (Fig. 7). The bistability threshold can be determined with a good precision by observing the spontaneous ''blinking'' between the two stable values, due to the intensity fluctuations or mechanical vibrations of optic elements on the setup. In the case of Fig. 7 $I_{thr}^{in} = 2.8$ mW.

Bistability threshold

The variations of the bistability threshold with the cavity-exciton detuning are shown in Fig. 9. We did not use any spatial filter here.

In the context of our previous assumption of small independent pixels, a precise calculation of the bistability threshold is not possible; the model predicts that each pixel of the excitation spot has its own bistability threshold. However, we can make a crude estimate by assuming that bistability occurs as soon as the local density of excitation in the center of the spot exceeds the bistability threshold calculated in Eq. (24). As a result, we have to divide the threshold (24) by the ratio of the local density at the center of the spot by the mean density of excitation, which is found to be $\sqrt{2}$.

The value of the nonlinear coefficient α_p is calculated using expression (16) with the measured spot diameter of $d_{spot} = 38 \pm 4$ μm. The polariton linewidth γ_p is estimated from a reflectivity measurement at $\delta = 1.5$ meV, which must be taken at threshold because the linewidth increases with the excitation density due to collision broadening. For the sake of simplicity, we have neglected the variations of γ_p in the considered range of cavity-exciton detunings (inferior to 10%). The solid line in Fig. 9 is the result of the model. It is in fair agreement with the experimental curve. As an illustration, error bars have been added for the point on the theoretical curve at $\delta = 1.5$ meV corresponding to the uncertainties in measuring the parameters of the fit α_{exc} and γ_p.

The general shape of the curve corresponds to the expected behavior. In particular, the minimal threshold is obtained at slightly positive detuning, near the theoretical value. However, as the detuning goes down to zero the

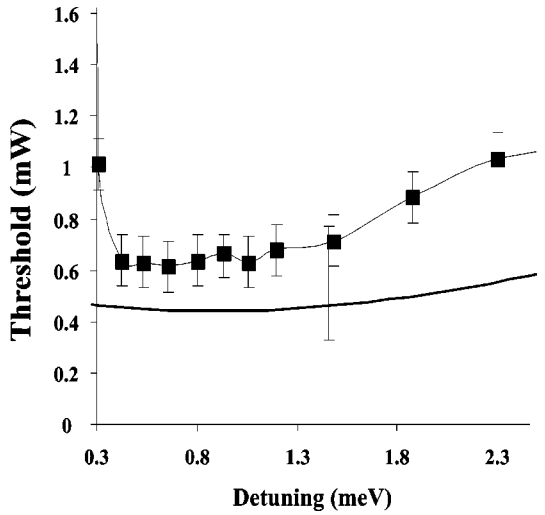

FIG. 9. Bistability threshold vs exciton-cavity detuning. Squares: experimental data (the line is a guide for the eyes). Solid line: theoretical curve calculated from the measured values of $d_{spot} = 38$ μm and $\gamma_p = 0.125$ meV. We added an error bar on the point at $\delta = 1.5$ meV of the theoretical curve showing the uncertainty on the theoretical value coming from the uncertainty in the measurement of the spot size and the polariton linewidth.

threshold intensity goes up very quickly (for example, it is superior to 25 mW for $\delta = 0.3$ meV). The origin of this discrepancy is yet to be understood. Transverse effects might play a key role, since the size (see Refs. [7,19]) and the shape of the polariton mode depend on the cavity-exciton detuning. As shown by the near-field images of the excitation spot, the polariton mode size is further reduced and its shape is altered, due to the angle between the cavity mirrors (see also Ref. [20] for a discussion of this effect), nonlinearities, and disorder. All these effects are also dependent on the cavity-exciton detuning, which might explain the brutal variations of the bistability threshold with detuning. A more elaborate model including the transverse mode structure of the polariton resonance and diffraction is likely to give new insights.

IV. CONCLUSION

We have reported, to our knowledge, the first observation of polaritonic bistability in semiconductor microcavities. It is obtained in the context of parametric polariton interaction in the degenerate case, where only the pumped mode at $k = 0$ is involved. A simple model treating the nonlinearity as a Kerr-type one gives a relatively good agreement with the experimental results. The originality of the bistable behavior reported here is that it occurs in the strong-coupling regime: the effective refraction index depends on the polariton number instead of the photons number. Moreover, it is well known that Kerr media can be used for the production of squeezed states of light. In the same way, this nonlinear mechanism can be used to produce squeezed states of the mixed light-matter polariton field [10,21].

ACKNOWLEDGMENT

We thank Romuald Houdré for providing us with the microcavity sample.

[1] C. Weisbuch *et al.*, Phys. Rev. Lett. **69**, 3314 (1992).
[2] R. Houdré *et al.*, C. R. Acad. Sci., Ser IV: Phys., Astrophys. **3**, 15 (2002), and references therein.
[3] G. Khitrova *et al.*, Rev. Mod. Phys. **71**, 1591 (1999).
[4] R. Houdré *et al.*, Phys. Rev. B **52**, 7810 (1995).
[5] A. Tredicucci, Y. Chen, V. Pellegrini, M. Börger, and F. Bassani, Phys. Rev. A **54**, 3493 (1996).
[6] P.G. Savvidis *et al.*, Phys. Rev. Lett. **84**, 1547 (2000); R.M. Stevenson *et al.*, *ibid.* **85**, 3680 (2000).
[7] J.J. Baumberg *et al.*, Phys. Rev. B **62**, R16 247 (2000).
[8] Le Si Dang, *et al.*, Phys. Rev. Lett. **81**, 3920 (1998); P. Senellart *et al.*, Phys. Rev. B **62**, R16 263 (2000); R. Butté *et al.*, *ibid.* **65**, 205310 (2002).
[9] G. Messin, J.Ph. Karr, A. Baas, G. Khitrova, R. Houdré, R.P. Stanley, U. Oesterle, and E. Giacobino, Phys. Rev. Lett. **87**, 127403 (2001).
[10] J.Ph. Karr, A. Baas, R. Houdré, and E. Giacobino, e-print cond-mat/0305106.
[11] C. Ciuti, P. Schwendimann, B. Deveaud, and A. Quattropani, Phys. Rev. B **62**, R4825 (2000).
[12] C. Ciuti, P. Schwendimann, and A. Quattropani, Phys. Rev. B **63**, 041303(R) (2001).
[13] B.G. Sfez, J.L. Oudar, J.C. Michel, R. Kuszelewicz, and R. Azoulay, Appl. Phys. Lett. **57**, 324 (1990).
[14] S. Pau, G. Bjrk, J.M. Jacobson, H. Cao, and Y. Yamamoto, Phys. Rev. B **51**, 14437 (1995).
[15] J.J. Hopfield, Phys. Rev. **112**, 1555 (1958).
[16] C. Ciuti, V. Savona, C. Piermarocchi, A. Quattropani, and P. Schwendimann, Phys. Rev. B **58**, 7926 (1998).
[17] See, for example, *Quantum Optics*, edited by D. F. Walls and G. J. Milburn (Springer-Verlag, Berlin, 1994).
[18] A. Lambrecht, J.M. Courty, S. Reynaud, and E. Giacobino, Appl. Phys. B: Lasers Opt. **60**, 129 (1995).
[19] G. Björk, H. Heitmann, and Y. Yamamoto, Phys. Rev. A **47**, 4451 (1993).
[20] G. Cassabois *et al.*, Phys. Rev. B **59**, R10 429 (1999).
[21] This model will be extended in a forthcoming paper to include quantum fluctuations in order to understand how squeezing can be achieved.